IEEE Access
Multidisciplinary ⋮ Rapid Review ⋮ Open Access Journal

Received 4 October 2022, accepted 18 November 2022, date of publication 30 November 2022,
date of current version 5 December 2022.

Digital Object Identifier 10.1109/ACCESS.2022.3225641

RESEARCH ARTICLE

Beamforming Algorithm Based on the Orthogonal Phase Bases With Trigonometric Estimation for Microwave Power Transfer Systems

HYUNGMO KOO[1], JAEKYUNG SHIN[2,3], WOOJIN CHOI[2,3], SOOHYUN BIN[2], HANSIK OH[1], HONGJUN LIM[2], KANG-YOON LEE[2], (Senior Member, IEEE), KEUM CHEOL HWANG[2], (Senior Member, IEEE), AND YOUNGOO YANG[2,3], (Senior Member, IEEE)

[1]Samsung Electronics Company Ltd., Yeongtong, Suwon 16677, South Korea
[2]Department of Electrical and Computer Engineering, Sungkyunkwan University, Suwon 16419, South Korea
[3]para-PA Inc., Suwon 16419, South Korea

Corresponding author: Youngoo Yang (yang09@skku.edu)

This work was supported by the Institute of Information and Communications Technology Planning and Evaluation (IITP) Grant through the Korea Government (MSIT), Development of low power/low delay/self-power suppliable RF simultaneous information and power transfer system and stretchable electronic epineurium for wireless nerve bypass implementation, under Grant 2020-0-00261.

ABSTRACT Microwave power transfer (MPT) has been widely studied, as sensors or mobile/wearable devices have been used, especially for IoT applications. A beamforming algorithm is essential and important for both the performance and the system complexity of MPT systems. In this paper, a beamforming algorithm that requires only $3N-2$ transmission sequences for the Tx array with N elements to estimate the optimum set of the transmission phases is proposed. The proposed algorithm is simply based on trigonometric calculations, and can be directly applied to an MPT system without element calibration. Calculation of the optimum phase set of the Tx only requires the information of the received power level from the Rx. Since simultaneous phase shifting of the multiple elements is performed during the power transmission sequence, it can have a relatively high Rx SNR, compared to the methods based on phase shifting of only one element at each sequence. In addition, optimum transmission phase sets for multiple Rx's can be obtained from a beamforming procedure using the proposed algorithm, if the received power levels from the multiple Rx's are collected. For verification of the proposed algorithm, a 5.2 GHz 8×4 Tx array having an output power of 0.5 W per Tx element was implemented. Beamforming experiment was performed using the proposed algorithm. A received power of 45 mW at 2 m distance was achieved, which is very close to the simulated value.

INDEX TERMS Microwave power transfer, channel estimation, phased array calibration, beamforming algorithm.

I. INTRODUCTION

Various sensors and mobile/wearable devices are being increasingly used for internet–of–things (IoT) systems. Additionally, various more sensors and implantable devices for automotive, industrial, or biological applications will be adopted. Because these devices require relatively low operating power, long-range wireless charging can be considered for convenience, rather than the conventional wired or short-range wireless charging methods. The MPT method has been studied for long-range wireless charging applications for these devices [1], [2], [3], [4], [5], [6], [7], [8], [9], [10], [11], [12], [13], [14], [15], [16], [17], [18]. Since the MPT method uses electromagnetic wave for power transmission, adaptive beamforming using a phased array is generally adopted to increase the power transmission efficiency, and

The associate editor coordinating the review of this manuscript and approving it for publication was Davide Comite.

to track the Rx's. For maximum received power at the Rx, it is necessary to estimate the channel characteristics between each Tx element and the Rx. Then, the optimum phase set for the Tx elements should be extracted for maximum power transmission.

The retroreflective beamforming method uses a pilot signal transmitted from the Rx to estimate the optimum phase set for the Tx channels to the Rx [9], [10], [11], [19], [20]. Since the phase of the pilot that arrives at each Tx element indicates the phase of the channel, transmitting the signal with a negative phase to that of the arrived pilot for each Tx element guarantees the maximum received power. The retroreflective beamforming is fast and straightforward, but requires an additional Tx in the Rx and Rx's in the Tx for pilot transmission and reception, respectively. The extra power consumption and cost for the pilot generation and transmission at the Rx is not desirable, especially for IoT devices that require low power consumption.

The look–up table (LUT) method is an alternative method that does not require pilot transmission and reception for channel estimation. An LUT that stores the channel information or the phase sets for the Tx elements that can be estimated using calculations, simulations, or measurements for various fixed locations of the Rx should be generated a priori [12], [13]. The optimum phase set should be adaptively searched for maximum power reception at the Rx. If the resolution of the table is insufficient, there could be a loss of received power. Since the real–time channel characteristics cannot be contained in the LUT, the estimated transmission phase may differ from the optimum as well. In addition, all the Tx elements should be accurately calibrated. Calibration of the Tx array may also be very complex and time–consuming [21], [22], [23], [24], [25], [26], [27], [28], [29], [30], [31], [32], [33], [34]. Even with fine calibration, drift in time or aging of the Tx elements can cause inaccuracy in beamforming, which results in a loss of the received power as well. Therefore, it is desirable for the beamforming algorithm to find the optimum phase set for the Tx elements without requiring complex calibration procedure or additional hardware.

II. BEAMFORMING ALGORITHMS FOR THE MPT

In general, far–field calibration methods can be used for the far–field beamforming method for the phased arrays [21], [22], [23], [24], [25], [26], [27], [28], [29], [30]. One of the most well–known far–field methods is the rotating element electric vector (REV) method [21]. While all the Tx elements are transmitting signals, rotating the phase of a single Tx element in all directions results in a sinusoidal variance of the received power. Using the phases for the maximum and minimum values of these sinusoidal received power levels, a relative complex gain of each channel for the specific Tx element can be obtained. This process should be repeated one–by–one for the entire Tx array. Since this classic REV method requires a large number of measurements, modified REV methods were proposed to obtain the complex gains of the channels by measuring only some specific phase shifting states for each Tx element [22], [23]. REV–based beamforming algorithms are very intuitive and simple, because they only need the received power levels to obtain complex gains from the element vectors. However, since as the number of array elements increases, the variation in the received power levels due to the phase shifting for a single Tx element becomes smaller, it becomes more and more difficult to secure a sufficient signal–to–noise ratio (SNR) of the Rx to accurately distinguish the variation of the received power levels according to the phase shifting states. Therefore, it could be ineffective to use these methods in a large Tx array. In addition, ambiguity from two solutions with plus and minus signs can exist for some modified versions of the REV methods. To remove this ambiguity, additional measurement should be performed, or a certain initial condition should be satisfied [21].

Some adaptive beamforming algorithms based on perturbation of the beam weight according to the received signal strength (RSS) were reported [14], [15], [16]. The beam weight should be corrected to the direction to increase the RSS. These algorithms do not require complex computation, extra hardware for the pilot signal, or additional calibration process. In addition, different from LUT methods, the system can dynamically optimize the transmission phases for real–time channel characteristics. To adjust the beam weight, a simple adaptation algorithm with a fixed perturbation step size for each element was proposed [14], [15]. To reduce the number of measurements required for convergence, adjusting the step size of perturbation according to the magnitude variation of the RSS was proposed [16], [35]. The algorithm reported in [17] solves a nonlinear least square problem using Levenberg–Marquardt method. The received power after each iteration gradually approaches to the maximum RSS point from randomly produced samples. Since these algorithms are based on the phase perturbation for a single element at a time, the same SNR issue can arise for large number of array elements as addressed for the REV-based methods. The SNR issue can be mitigated by simultaneously rotating the phases of the multiple Tx elements. Reference [24] shifted the phases of the multiple elements with a specified phase interval, and their individual field properties could then be obtained using the Fourier series. However, since the number of elements for simultaneous phase shift and the control bits for the phase shifter are limited, the number of required measurements cannot be significantly reduced, as reported in [22] and [23].

Unlike the conventional REV, [25] proposed that all the array elements are combined in two groups using the Hadamard matrix. Phase shifting with angles of 0°, 90°, and 180° are performed for the grouped elements. The relative magnitude and phase of each group are obtained using the trigonometric properties. Then, the characteristics of each element are extracted through the calculation using matrix inversion. Although the number of measurements can be remarkably reduced compared to the conventional methods, and the robustness of the SNR of the Rx can be improved,

TABLE 1. Beamforming methods for the MPT.

Classification	Features	Pros	Cons	References
Retroreflective	Signal generator and Tx for the pilot signal at the Rx	Very fast channel estimation	Complex hardware Accurate calibration for the Tx elements	[9–11], [19, 20]
Look-up table	Tabularized optimum Tx phase sets	Fast channel estimation Simple hardware	Hard to follow the hardware variations over time and the real–time channel characteristics Accurate calibration for the Tx elements	[12, 13]
REV	Min/Max measurement for the received power levels by rotating each element vector for all possible phase angles	Straightforward	Low Rx SNR Large number of measurements Ambiguity in polarity Ineffective for large array	[21]
Modified REV for specific phase angles	Measurement for the received power levels by rotating each element vector by 0°, 90°, 180° and 270° (4 states)	Reduced number of measurements : ($3N$+1)	Low Rx SNR Ineffective for large array	[22]
	Measurement for the received power levels by rotating each element vector by 0°, 90° and 180° (3 states)	Reduced number of measurements : ($2N$+1)	Low Rx SNR Ineffective for large array Ambiguity in polarity	[23]
Adaptive tracking based on RSS	Perturbation on beam weight for each element Positive gradient tracking for the received power	Adaptive operation	Low Rx SNR Large number of measurements Ineffective for large array	[14]–[17]
Simultaneous rotation of the multiple element vectors based on the orthogonal phase bases	Measurements for the received power levels by simultaneously rotating multiple element vectors by 0°, 90° and 180° (3 states) REV-based estimation Element grouping using the orthogonal matrix	High Rx SNR Single beam sequence for multiple Rx's Number of measurements : ($3N$)	Ambiguity in polarity	[25]
	Perturbation on beam weights of the multiple elements Positive gradient tracking along with the orthogonal phase bases Element grouping using the orthogonal matrix	High Rx SNR Adaptive operation	No finite number of measurements	[18]
	Measurements for the received power levels by simultaneously rotating multiple element vectors for 0°, 90° and power on/off (4 states) Trigonometric estimation of the optimum phase set Element grouping using the orthogonal matrix	High Rx SNR Single beam sequence for multiple Rx's Number of measurements : ($3N$-2)	–	This work

it still has the ambiguity issue, like the conventional REV. The algorithm reported in [18] also uses the Hadamard matrix to divide the entire array into two groups with $N/2$ elements. Then, N orthogonal phase masks are generated, and used to determine the phase shifting direction of each element. The optimum transmission phase of each element can be derived using the orthogonality of the transmission phase sets. The adaptive beamforming algorithm finds the optimum phase set to have the maximum received power with each orthogonal phase mask. This technique is insensitive to hardware errors, because perturbation of the transmission phase occurs in the direction of increasing RSS.

Especially for the IoT applications, the capability of multiple device charging is also very important for the MPT methods. If the next beam weight can be determined using the RSS information for the current beam, or if the optimum

phase set should be adaptively tracked, the beamforming process must be performed only for a single Rx. If the beamforming sequence is not dependent on the state of the Rx [22], [23], [25], the optimum transmission phase set for each Rx can be simultaneously obtained from the RSS's of the multiple Rx's.

In this paper, a beamforming algorithm for MPT systems is proposed that does not require a calibration process for the Tx elements, but does require a lesser number $(3N-2)$ of beams for the transmission sequence to find the optimum phase set for the Tx elements. For the Tx array with N elements, the proposed algorithm uses an $N\times N$ Hadamard matrix to make N bases for simultaneous phase shifting of multiple elements. To find the optimum transmission phase set using the N bases, a transmission sequence with $3N-2$ beams, which consist of 0°, 90°, and power–off states for the elements, is required. After the measurement for the transmission sequence, the optimum transmission phase of each Tx element for a given Rx location can be calculated using trigonometric geometry and orthogonality. Since simultaneous phase shifting for half of the Tx elements is performed, this technique has a relatively high Rx SNR, compared to the algorithms based on phase shifting of a single Tx element at a time or RSS variations as in [14], [15], [16], [17], [21], [22], and [23]. Unlike [14], [15], [16], [17], and [35], the proposed algorithm generates the $3N-2$ beams with phases of 0°, 90°, and power–off states of other elements, so that if the received power levels of the multiple Rx's are determined, optimum phase sets for the multiple Rx's can be simultaneously obtained using a single beam sequence. Compared to the methods presented in [21], [23], and [25], the procedure is simple, without requiring initial conditions. Table 1 summarizes the pros and cons of the proposed and previously reported beamforming algorithms.

III. THE PROPOSED BEAMFORMING ALGORITHM

A. HADAMARD GROUPING FOR MULTI–ELEMENT PHASE SHIFTING

The transmitted field from the N Tx elements arrives at the receiving antenna through the wireless channels. Each channel between each Tx element and the Rx can be expressed as a complex gain. The vector matrix of the N wireless channels for the N Tx elements is expressed as follows:

$$\boldsymbol{g} = \left[A_{g,1}e^{j\theta_{g,1}}\ A_{g,2}e^{j\theta_{g,2}}\ \cdots\ A_{g,N}e^{j\theta_{g,N}}\right], \tag{1}$$

where $A_{g,i}$ and $\theta_{g,i}$ are the magnitude and phase of the complex gain for the i–th channel. It can be assumed that the output power levels of the Tx elements are the same, since the output power from each Tx element should be its peak output power to receive the maximum power at the Rx for MPT systems. Therefore, for the Tx elements operating with the peak output power, the receive field, r, can be simply calculated as follows:

$$r = \boldsymbol{g}\boldsymbol{x}^{\mathrm{T}} = E_0\sum_{k=1}^{N} A_{g,k}e^{j(\theta_{g,k}+\theta_{x,k})}, \tag{2}$$

where $\boldsymbol{x}$ is a beam weight for the N Tx elements, and can be represented using a vector matrix, as follows:

$$\boldsymbol{x} = E_0\left[e^{j\theta_{x,1}}\ e^{j\theta_{x,2}}\ \cdots\ e^{j\theta_{x,N}}\right], \tag{3}$$

where E_0 is the magnitude of the beam weight for the same output power, and $\theta_{x,i}$ is the phase of the beam weight for the i–th channel. From Eq. (2), it can be found that the received field is dependent on the phases, $\theta_{x,1}$ to $\theta_{x,N}$, of the transmitted signals from the Tx elements. It can be also found that the received field can be maximized when the sum of the two phases of the complex gain and the transmitted signal from the i–th Tx element to the Rx becomes the same constant value, or simply zero, for all the Tx elements.

To find the maximum received power point, one of the most intuitive methods is a gradient algorithm that is continuously chasing toward the positive gradient of the function along the coordinate axis. For N–dimensional functions, N orthogonal bases are required to run such max point searching algorithms. Since the axes of the transmission phase of single Tx element are not orthogonal each other, the method of sequentially rotating the individual phase of the transmitted signal from each Tx element could not always lead to the global optimum, and might require too many measurements. In addition, as the number of Tx array increases, the received power variation according to the phase change of a single element becomes smaller, and could even be difficult to correctly detect, due to the relatively low signal level compared to the noise level. In other words, this method can have a low SNR issue at the Rx, especially for large Tx array.

If orthogonal bases for N–dimensional phases are found and simultaneous phase shift in multiple elements can be performed, the global optimum point with a relatively large Rx SNR can be found. To make N orthogonal basis vectors, the Hadamard matrix has been popularly used. The $2^m\times 2^m$ Hadamard matrix with orthogonal bases is represented as follows:

$$\boldsymbol{H}_2 = \begin{bmatrix} 1 & 1 \\ 1 & -1 \end{bmatrix}, \tag{4}$$

$$\boldsymbol{H}_{2^m} = \begin{bmatrix} \boldsymbol{H}_{2^{m-1}} & \boldsymbol{H}_{2^{m-1}} \\ \boldsymbol{H}_{2^{m-1}} & -\boldsymbol{H}_{2^{m-1}} \end{bmatrix}, \tag{5}$$

where m is an integer. Then, the $N\times N$ Hadamard matrix for N Tx elements can be represented as follows:

$$\boldsymbol{H}_N = \begin{bmatrix} h_{11} & \cdots & h_{11} \\ \vdots & \ddots & \vdots \\ h_{N1} & \cdots & h_{NN} \end{bmatrix}. \tag{6}$$

For the Tx array having 2^m elements, all the even rows and columns have the same number of appearances for the values of 1 and -1, except row 1 and column 1. Values of 1 and -1

in the matrix indicate the positive and negative direction of the phase shift, respectively. If the phase shift directions of the elements for a selected row are defined, N basis vectors with simultaneous phase shift of the N Tx elements can be created for the vector matrix $\boldsymbol{x}$. Then, the phase set for the maximum received power can be found through these new basis vectors. The new vector matrix of the beam weight, $\boldsymbol{u}$, with these orthogonal bases of the phases for the array with N or 2^m elements, can be defined using the elements of the Hadamard matrix, as follows:

$$\boldsymbol{u}_n = E_0 \left[e^{jh_{n1}\theta_{x,n}} \; e^{jh_{n2}\theta_{x,n}} \; \cdots \; e^{jh_{nN}\theta_{x,n}} \right], \tag{7}$$

where $\boldsymbol{u}_n$ is the vector matrix of the beam weight made from the n–th row of the Hadamard matrix. According to Eq. (7), if the phase of the existing beam weight is multiplied by -1, the element has a phase shift to the opposite direction, compared to the direction of the phase shift from multiplication by 1. This means that for the same phase shift angle of θ, $N/2$ elements transmit signals with a transmission phase of $+\theta$, while the other $N/2$ elements transmit signals with a transmission phase of -θ. Then, the matrix $\boldsymbol{r}$ for the received fields based on N basis vectors for the phases are defined as follows:

$$\boldsymbol{r} = \left[r_1 \; r_2 \; \cdots \; r_N \right], \tag{8}$$

where the n–th element, r_n, is the received field for the beam weight of $\boldsymbol{u}_n$ and can be expressed as follows:

$$\boldsymbol{r}_n = \boldsymbol{g}\boldsymbol{u}_n{}^{\mathrm{T}} = E_0 \sum_{k=1}^{N} A_{g,k} e^{j(\theta_{g,k} + h_{nk}\theta_{x,k})}. \tag{9}$$

To find the optimal transmission phases of the Tx elements, we have to find $\theta_{x,n}$, which maximizes the received field, r_n. This optimum phase searching should be done for all n from (1 to N). Using the optimum transmission phase, $(\theta_{x,n})_{opt}$ for $\boldsymbol{r}_n$ to be the maximum received field gives the expression for the optimum beam weight, as follows:

$$\boldsymbol{x}_{opt} = E_0 \Bigg[\sum_{k=1}^{N} e^{jh_{k1}(\theta_{x,k})_{opt}} \quad \sum_{k=1}^{N} e^{jh_{k2}(\theta_{x,k})_{opt}} \quad \cdots \quad \sum_{k=1}^{N} e^{jh_{kN}(\theta_{x,k})_{opt}} \Bigg]. \tag{10}$$

Using Eq. (10), the optimum transmission phases are obtained. Since all elements have the same phase shift direction in $\boldsymbol{r}_1$, the same received power for all possible phase settings can only be obtained, so that the phase, $(\theta_{x,1})_{opt}$, for the maximum value cannot be obtained. However, since $(\theta_{x,1})_{opt}$ is equally added to the optimum phases of all the Tx elements as in Eq. (10), it does not make any relative phase difference. Therefore, $(\theta_{x,1})_{opt}$ can be ignored with a value of zero. How to find $(\theta_{x,n})_{opt}$ has been one of the key issues. The proposed method will be explained in the next subsection.

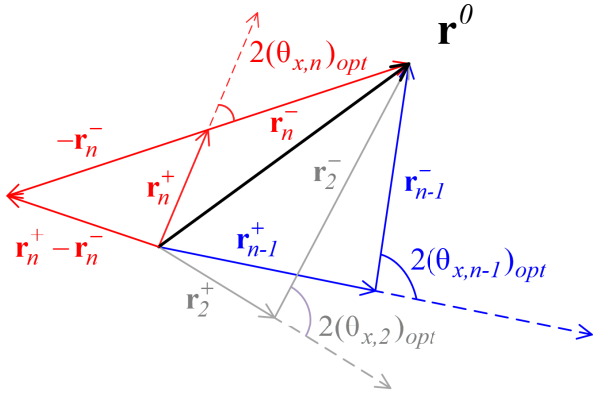

FIGURE 1. Vector diagram of the received field with an initial beam weight.

B. OPTIMUM PHASE ESTIMATION

If the same phase shift is applied to all the vector components, the same phase shift occurs in the composite vector as well. The $\boldsymbol{r}_n$ in Eq. (9) is N summations of vectors, each of which has a phase shift with + or - direction. Therefore, by grouping vectors having the same phase shift direction according to the new beam weight in Eq. (7), $\boldsymbol{r}_n$ can be re–expressed as a sum of two vectors: a vector, $\boldsymbol{r}_n^+$, from the received fields for the elements that have phase shift in the + direction, and a vector, $\mathbf{r}_n^-$, from the received fields for the elements that have phase shift in the - direction. Then, Eq. (9) can be rewritten as follows:

$$\boldsymbol{r}_n = \boldsymbol{r}_n^+ + \boldsymbol{r}_n^- = E_0 \Bigg\{ \sum_{k=1}^{N} A_{g,k} \frac{1 + h_{nk}}{2} e^{j(\theta_{g,k} + \theta_{x,n})} + \sum_{k=1}^{N} A_{g,k} \frac{1 - h_{nk}}{2} e^{j(\theta_{g,k} - \theta_{x,n})} \Bigg\}, \tag{11}$$

where n is an integer from (1 to N). Since $\boldsymbol{r}_n^+$ and $\boldsymbol{r}_n^-$ have a phase shift in opposite directions, they can be combined in–phase to result in a maximum magnitude if they have exactly half phase shift of the initial phase difference. Therefore, the optimum transmission phase $(\theta_{x,k})_{opt}$ in Eq. (10) should be half of the phase difference between the two vectors, $\boldsymbol{r}_n^+$ and $\boldsymbol{r}_n^-$, which are expressed in Eq. (11). For the initial state with no phase shift (i.e., $\theta_{x,n}$ of 0 in Eq. (11)), all the $\boldsymbol{r}_n$'s for any value of n are the same vector. Though the phase difference between the two vector components shown in Eq. (11) varies according to n with the initial condition of zero phase shifting, their vector sum becomes always the same.

Fig. 1 indicates the vector diagram for the case with no phase shift. Here, $\boldsymbol{r}^0$ is the received field using the transmitted signal for an initial beam weight with no phase shifting. $\boldsymbol{r}_n^+$ and $\boldsymbol{r}_n^-$ can be simply acquired by turning on the elements having the desired sign of phase shifting direction, and turning off the elements that do not. If the magnitude of the received fields, $\boldsymbol{r}^0$, $\boldsymbol{r}_n^+$ and $\boldsymbol{r}_n^-$ are known, it may be possible to

estimate $(\theta_{x,n})_{opt}$ simply using a cosine law. However, since the cosine function is an even function, it is still not clear whether $(\theta_{x,k})_{opt}$ is positive or negative. A simple way to avoid this ambiguity of the sign of the phase is to measure the received power using either a positive or negative phase value. If the chosen polarity of the phase is correct to have an in–phase combination of $\boldsymbol{r}_n^+$ and $\boldsymbol{r}_n^-$, a field larger than $\boldsymbol{r}^0$ will be obtained. The received power will be increased as well. If it is incorrect, the received power will decrease. If this method is applied to the condition with multiple Rx's in different locations, each Rx requires a different transmission phase set to determine the sign of the phase. Therefore, for the method using a simple cosine law, the measurements using a different beam sequence should be applied to each Rx, so that the number of required measurements increase in proportion to the number of Rx's.

To simultaneously estimate the optimum transmission phase sets for the multiple Rx's with a single unified beam sequence, the received power levels of $P_n^{\pi/2}$ and P_n^{π} with phase shifts of $\boldsymbol{r}_n^-$ by 90° and 180°, respectively, can be used. Using the new beam weight setting in Eq. (7), phase shifts of 45° and 90° can make relative phase differences of 90° and 180° between $\boldsymbol{r}_n^+$ and $\boldsymbol{r}_n^-$. For convenience, the phase of $\boldsymbol{r}_n^-$ can be represented using the phase of $\boldsymbol{r}_n^+$ as a reference. The relative received power levels for $\boldsymbol{r}_n^+$ and $\boldsymbol{r}_n^-$ and their combinations with phase shifts can be simply expressed as follows:

$$P_n^+ = |\boldsymbol{r}_n^+|^2, P_n^- = |\boldsymbol{r}_n^-|^2, \tag{12}$$
$$P^0 = |\boldsymbol{r}^0|^2 = |\boldsymbol{r}_n^+ + \boldsymbol{r}_n^-|^2, \tag{13}$$
$$P_n^{\pi} = |\boldsymbol{r}_n^+ - \boldsymbol{r}_n^-|^2, \tag{14}$$

where, P_n^+, P_n^-, and P^0 are the relative received power levels for $\boldsymbol{r}_n^+$, $\boldsymbol{r}_n^-$, and $\boldsymbol{r}^0$, respectively. Note that P^0 is a constant that is independent of n, which is the index of the row for the Hadamard matrix used to define Eq. (7), while P_n^{π} are different according to n. From Eqs. (12)–(14), the following equations can be derived using vector geometry:

$$P_n^+ + P_n^- = \frac{1}{2}(P^0 + P_n^{\pi}). \tag{15}$$

Eq. (15) shows that P_n^{π} can be derived using the received power levels of P_n^+, P_n^-, and P^0. Then, from the vector diagram shown in Fig. 1, the optimum phase, $(\theta_{x,n})_{opt}$, for the n–th phase basis can be derived using the cosine law, as follows:

$$(\theta_{x,n})_{opt} = \pm\frac{1}{2}cos^{-1}\left(\frac{P_n^+ + P_n^- - P_n^{\pi}}{2\sqrt{P_n^+ P_n^-}}\right) = \pm\frac{1}{2}cos^{-1}\left(\frac{P^0 - P_n^+ - P_n^-}{2\sqrt{P_n^+ P_n^-}}\right), \tag{16}$$

while the magnitude of the optimum phase for each phase basis can be found using Eq. (16), the correct sign should still be found. To find the correct sign, the relationships between P^0, $P_n^{\pi/2}$, and P_n^{π} should be observed.

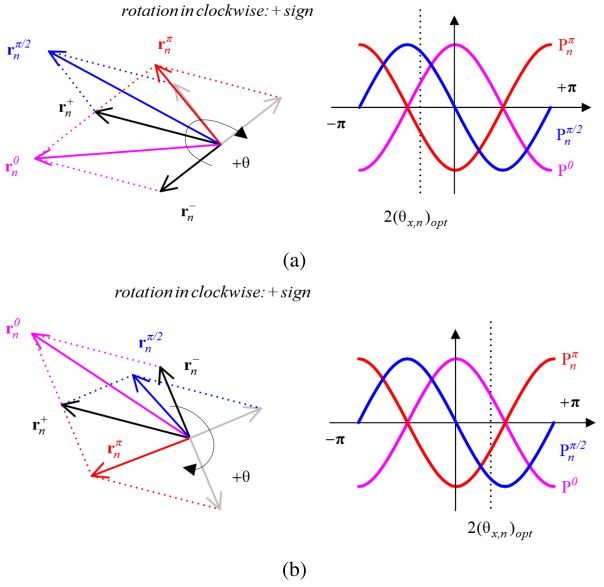

FIGURE 2. Vector diagram and signal waveforms to find the sign of the optimum phase based on magnitude comparison: (a) lagging, and (b) leading.

TABLE 2. Relationships between P^0, $P_n^{\pi/2}$, and P_n^{π} with respect to the ranges of $2(\theta_{x,n})_{opt}$.

Phase range	Relationships
$-\pi \le 2(\theta_{x,n})_{opt} < -3\pi/4$	$P^0 < P_n^{\pi/2} < P_n^{\pi}$, $P_n^{\pi} - P_n^{\pi/2} < P_n^{\pi/2} - P^0$
$-3\pi/4 \le 2(\theta_{x,n})_{opt} < -\pi/2$	$P^0 < P_n^{\pi} < P_n^{\pi/2}$
$-\pi/2 \le 2(\theta_{x,n})_{opt} < -\pi/4$	$P_n^{\pi} < P^0 < P_n^{\pi/2}$
$-\pi/4 \le 2(\theta_{x,n})_{opt} < 0$	$P_n^{\pi} < P_n^{\pi/2} < P^0$, $P^0 - P_n^{\pi/2} < P_n^{\pi/2} - P_n^{\pi}$
$0 \le 2(\theta_{x,n})_{opt} < \pi/4$	$P_n^{\pi} < P_n^{\pi/2} < P^0$, $P_n^{\pi/2} - P_n^{\pi} < P^0 - P_n^{\pi/2}$
$\pi/4 \le 2(\theta_{x,n})_{opt} < \pi/2$	$P_n^{\pi/2} < P_n^{\pi} < P^0$
$\pi/2 \le 2(\theta_{x,n})_{opt} < 3\pi/4$	$P_n^{\pi/2} < P^0 < P_n^{\pi}$
$3\pi/4 \le 2(\theta_{x,n})_{opt} < \pi$	$P^0 < P_n^{\pi/2} < P_n^{\pi}$, $P_n^{\pi/2} - P^0 < P_n^{\pi} - P_n^{\pi/2}$

Fig. 2 shows the vector diagram and signal waveforms to find the sign of the optimum phase based on magnitude comparison. The sign of the angle between $\boldsymbol{r}_n^+$ and $\boldsymbol{r}_n^-$ in Eq. (16) results in lagging (Fig. 2a) or leading (Fig. 2b) waveforms. These two cases show different relationships of P^0, $P_n^{\pi/2}$, and P_n^{π}. For example, for the case shown in Fig. 2a, where $\pi/4 < 2(\theta_{x,n})_{opt} < \pi/2$, P^0 is the largest. Otherwise, for the case shown in Fig. 2b, $P_n^{\pi/2}$ is the largest. All possible angles from $(-\pi$ to $+\pi)$ between $\boldsymbol{r}_n^+$ and $\boldsymbol{r}_n^-$ can be divided into 8 sections according to the relationships between P^0, $P_n^{\pi/2}$, and P_n^{π}, as shown in Table 2.

Table 2 shows that if the relationships between the 3 received power levels are compared, or if which one is

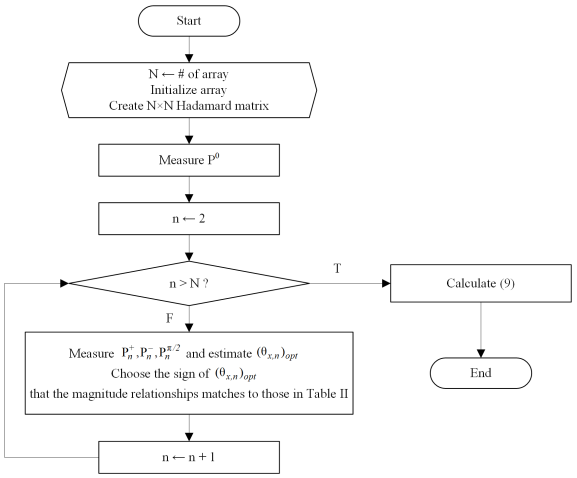

FIGURE 3. Flow chart of the proposed algorithm.

closer to the second largest value between other two received power levels is known, the correct sign in Eq. (16) can be determined after a single beam sequence. Since when n is 1, all the elements have the same phase shift, the maximum received power cannot be obtained. Therefore, measurements to find P_n^+, P_n^-, and $P_n^{\pi/2}$ are not required for n of 1. P_n^+, P_n^-, and $P_n^{\pi/2}$ should be measured, and P_n^π should be derived for all other n's from (2 to N). So the beam sequence for each element consists of power on/off state and two phase shift states of 0° and 90°. In addition, since P^0 is required to be measured, the total number of measurements by the beam sequence is $3N-2$. After the beam sequence, all the parameters in Table 2 are obtained. Two sections in Table 2 can be pre–selected using the absolute value of the optimum phase derived in Eq. (16). By examining the relationships between the measured P^0, $P_n^{\pi/2}$, and P_n^π, the correct sign of $(\theta_{x,n})_{opt}$ can be found. If all $(\theta_{x,n})_{opt}$'s for n of (1 to N) are obtained, the optimum transmission phases of the N Tx elements for the current position can be obtained using Eq. (10). Fig. 3 shows a brief flow chart of the proposed beamforming algorithm with the total number of measurements of only $3N-2$, without ambiguity of the sign of the optimum phase.

IV. SYSTEM DESIGN AND IMPLEMENTATION

A. SYSTEM DESIGN

For verification of the proposed algorithm, a 5.2 GHz MPT system including an 8 × 4 Tx array was designed. Fig. 4 shows the overall system block diagram. The Tx is composed of 8 × 4 or 32 elements. Each Tx element includes a power amplifier, a phase shifter, an attenuator, a micro controller unit (MCU), and an antenna. The phase shifter has a 5–bit control with a phase step of 5.625° for the entire coverage of 360°. The attenuator also has a 5–bit control with a step of 0.5 dB for the maximum attenuation level of 31.5 dB. The MCU's are connected to a PC via universal asynchronous receiver/transmitter (UART). The

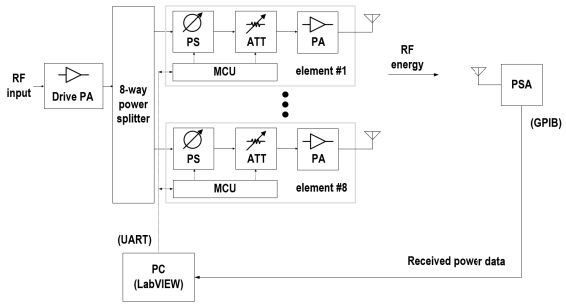

FIGURE 4. Block diagram of the MPT system.

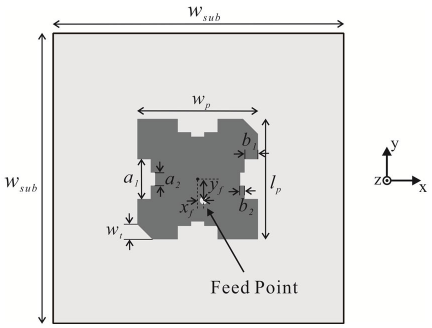

FIGURE 5. Patch antenna used for the Tx elements.

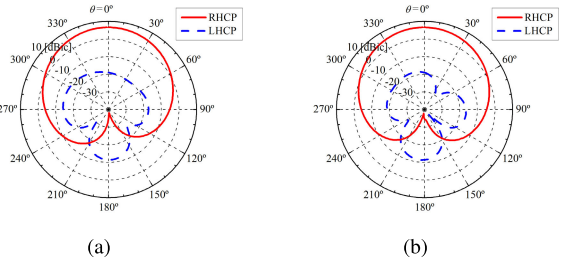

FIGURE 6. Simulated radiation patterns of the 5.2 GHz antenna element: (a) *xz*–plane, and (b) *yz*–plane.

algorithm was implemented using LabVIEW, and the beam sequences were uploaded on the MCUs. Table 3 summarizes the components used for the design.

Fig. 5 shows the Koch–curve structure–based patch antenna element for the Tx array [36]. The antenna element has a dimensions of 34 mm×34 mm×1.52 mm, and was implemented on RF–35 substrate with a dielectric constant of 3.5 and a loss tangent of 0.0018. Using the feed point located at distances of 0.7 mm in the x direction and 2.5 mm in the −y direction from the center and the cuts at two corners, a right–handed circular polarization (RHCP) was realized. The parameters of w_p, l_p, and w_t for the patch are (14.08, 14.08, and 1.75) mm, respectively. The parameters a_1, a_2, b_1, and b_2 are (w_p/3, w_p/9, w_p/9, and w_p/27), respectively.

Fig. 6 shows the simulated radiation patterns of the designed antenna element for the xz–plane in (a) and the yz–plane in (b). The RHCP gain is 6.5 dBic for the +z direction. The gain difference between RHCP and LHCP is about 25.65 dB at 5.2 GHz. The bandwidth for a reflection

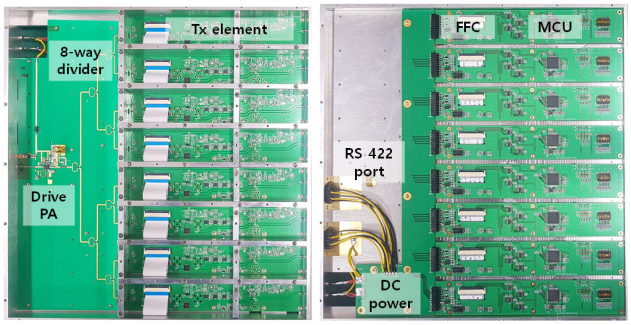

(a) (b)

FIGURE 7. Implemented 8 × 1 unit Tx array: (a) top view, and (b) bottom view.

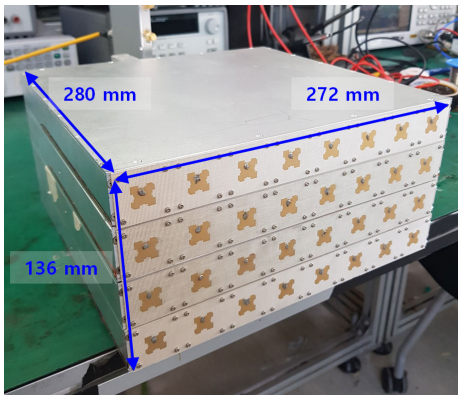

FIGURE 8. The implemented 8 × 4 Tx array.

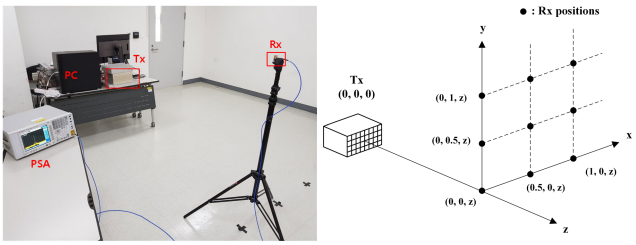

(a) (b)

FIGURE 9. (a) experimental setup for the MPT, and (b) Rx positions for the measurements.

coefficient of under −10 dB ranges from (5.05 to 5.29) GHz, which is 4.642%. The 8 × 4 antenna array with an interval of 0.59 λ_0 between the adjacent elements showed a high gain of 18.19 dBic. The same single antenna element is used for the Rx, and is connected to the power spectrum analyzer (PSA). The information of the measured received power levels for the $3N-2$ beam sequences is delivered back to the PC through the general purpose interface bus (GPIB). Based on the received power levels, the proposed algorithm calculates the optimum phase set for the Tx.

B. IMPLEMENTATION

Fig. 7 shows the photographs of the fabricated unit Tx array: (a) top view, and (b) bottom view for the 8 Tx elements. The RF circuits are implemented on the top plate of the board,

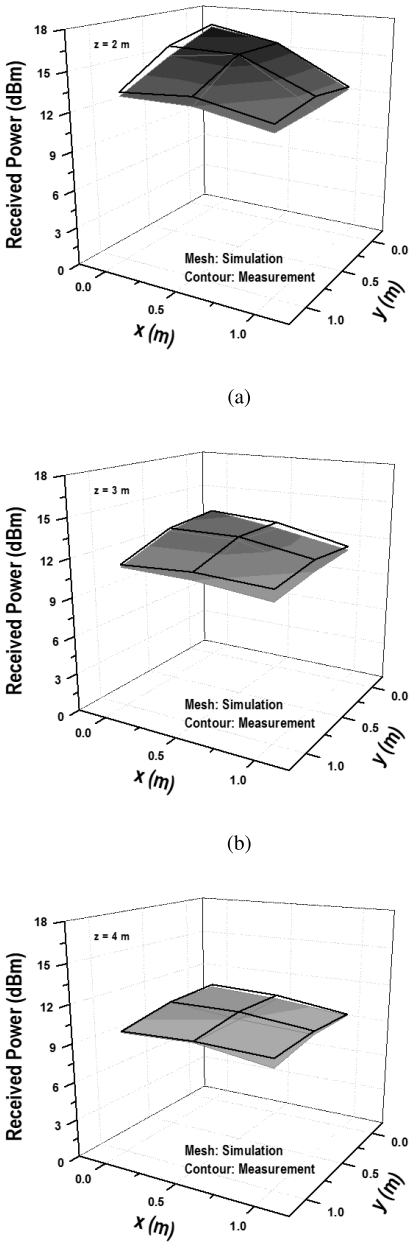

(a)

(b)

(c)

FIGURE 10. Simulated and measured received power levels for various Rx locations: (a) z = 2, (b) z = 3, and (c) z = 4 m.

while the digital and power management circuits, including MCU's and low drop–out IC's, are placed on the bottom. The top and bottom circuits are inter–connected using a flexible flat cable (FFC). Fig. 8 shows a photograph of the implemented 8 × 4 array. The entire array has dimensions of 272 mm×136 mm×280 mm.

V. MEASUREMENT RESULTS

Fig. 9a shows the experimental setup for MPT using the implemented Tx array and the proposed beamforming algorithm. Fig. 9b shows the locations of the Rx where the measurements were performed. Measurement planes were

TABLE 3. Summary of the measurement results compared to the previous MPT systems.

Ref.	Beamforming algorithm	Frequency (GHz)	# of Tx array	P_{OUT} (W/element)	P_{OUT} (W)	# of Rx antennas	P_R (W)	Distance (m)
[16]	Adaptive (Gradient ascent with weight optimization)	0.915	4	0.1	0.4	1	0.009* (RF)	1
[10]	Retroreflective	2.08	4	0.25	1	1	0.014 (RF)	0.5
[11]	Retroreflective	2.125	8	0.175	1.4	1	0.007 (RF)	0.6
[30]	Retroreflective	5.2	64	0.5	32	1	0.446 (RF)	1
						5	0.575 (dc)	
[12]	Look–up table	5.2	32	0.5	16	1	0.178 (RF)	1
						5	0.191 (dc)	
[14]	Adaptive (Gradient ascent)	5.2	32	0.5	16	1	0.229 (RF)	1
	Retroreflective						0.208 (RF)	
[13]	Look–up table	5.8	16	0.079	1.3	16	0.007* (RF)	4
[18]	Adaptive (Orthogonal phase bases with gradient ascent)	10	400	N/A	N/A	64	2 (DC)	1
This work	Proposed (Orthogonal phase bases with trigonometric estimation)	5.2	32	0.5	16	1	0.045 (RF)	2

*: Graphically estimated, N/A: not available

coordinated at the distances in the z axis (z = (2, 3, and 4) m) from the center of the Tx antenna array (reference point, z = 0). For each measurement plane, 9 Rx positions were selected for the measurements with spaces of 0.5 m along both the x and y axes. The output power of each Tx element was set as 27 dBm, which results in the total Tx power for the 32 elements of about 42 dBm. As introduced in section III, the proposed algorithm requires the information of the received power levels for a total 94 (or $3N-2$) beams to calculate the optimum Tx phase set for each Rx position:

Fig. 10 shows the simulated and measured received power levels for a total of 27 Rx locations, that is, 9 locations for each plane, where z is (2, 3, or 4) m. The received RF power levels of (16.6, 13.3, and 10.6) dBm were obtained at the line–of–sight positions with z's of (2, 3, and 4) m, respectively. The minimum received power levels were (12, 10.4, and 9) dBm for the three planes. The simulation was done using the method explained in [37]. The maximum difference of the received power levels between the measured and simulated results is only 0.9 dB. The very close match between the simulated and measured results validates the proposed beamforming algorithm. Table 4 summarizes the measured performances of this work, compared to the previously reported MPT systems. This work showed a received power of 45 mW at a relatively far distance of 2 m.

VI. CONCLUSION

In this paper, pros and cons for the features of the beamforming algorithms used for MPT systems were analyzed. A new algorithm which that requires no calibration routine for the Tx elements and requires no additional circuits, such as auxiliary Rx circuits for the Tx or auxiliary Tx circuits for the Rx, is proposed. Using the proposed algorithm, the optimum phase set for the Tx array can be obtained through the received power measurements using the $3N-2$ pre–coded beams. Since the received power measurement is done using the simultaneous phase shift for the multiple Tx elements, the MPT system based on this proposed algorithm has an improved Rx SNR. The entire beam sequence is generated using some fixed conditions, such as 0° and 90° phase shifts for all the Tx elements, and power on/off states of the partial Tx elements. Since the beam sequence is based on fixed conditions, the proposed beamforming algorithm enables the MPT system to simultaneously estimate the optimum Tx phase sets for multiple Rx's if the information of the received power levels from the multiple Rx's can be independently acquired at the Tx.

The operational principles of the proposed algorithm were explained simply using some trigonometric properties for the vectors. To verify the proposed algorithm, an MPT system based on an 8×4 Tx array was implemented for the 5.2 GHz

band. Each Tx element has an output power of 0.5 W. For the beamforming experiments using the implemented MPT system, a received power of 45 mW at the distance of 2 m distance was achieved. Superiority of the proposed algorithm was verified by the close match between the measured and simulated received power levels and the small number of measurements ($3N-2$) without ambiguity.

REFERENCES

[1] W. C. Brown, "The history of power transmission by radio waves," *IEEE Trans. Microw. Theory Techn.*, vol. MTT-32, no. 9, pp. 1230–1242, Sep. 1984.
[2] W. C. Brown and E. E. Eves, "Beamed microwave power transmission and its application to space," *IEEE Trans. Microw. Theory Techn.*, vol. 40, no. 6, pp. 1239–1250, Jun. 1992.
[3] H. Matsumoto, "Research on solar power satellites and microwave power transmission in Japan," *IEEE Microw. Mag.*, vol. 3, no. 4, pp. 36–45, Dec. 2002.
[4] A. Massa, G. Oliveri, F. Viani, and P. Rocca, "Array designs for long-distance wireless power transmission: State-of-the-art and innovative solutions," *Proc. IEEE*, vol. 101, no. 6, pp. 1464–1481, Jun. 2013.
[5] Q. Hui, K. Jin, and X. Zhu, "Directional radiation technique for maximum receiving power in microwave power transmission system," *IEEE Trans. Ind. Electron.*, vol. 67, no. 8, pp. 6376–6386, Aug. 2020.
[6] C. K. Wang, B. J. Xiang, S. Y. Zheng, K. W. Leung, W. S. Chan, and Y. A. Liu, "A wireless power transmitter with uniform power transfer coverage," *IEEE Trans. Ind. Electron.*, vol. 68, no. 11, pp. 10709–10717, Nov. 2021.
[7] E. Y. Chow, A. L. Chlebowski, S. Chakraborty, W. J. Chappell, and P. P. Irazoqui, "Fully wireless implantable cardiovascular pressure monitor integrated with a medical stent," *IEEE Trans. Biomed. Eng.*, vol. 57, no. 6, pp. 1487–1496, Jun. 2010.
[8] K. W. Choi, L. Ginting, A. A. Aziz, D. Setiawan, J. H. Park, S. I. Hwang, D. S. Kang, M. Y. Chung, and D. I. Kim, "Toward realization of long-range wireless-powered sensor networks," *IEEE Wireless Commun.*, vol. 26, no. 4, pp. 184–192, Aug. 2019.
[9] T. Takahashi, T. Sasaki, Y. Homma, S. Mihara, K. Sasaki, S. Nakamura, K. Makino, D. Joudoi, and K. Ohashi, "Phased array system for high efficiency and high accuracy microwave power transmission," in *Proc. IEEE Int. Symp. Phased Array Syst. Technol. (PAST)*, Oct. 2016, pp. 18–21.
[10] X. Wang, S. Sha, J. He, L. Guo, and M. Lu, "Wireless power delivery to low-power mobile devices based on retro-reflective beamforming," *IEEE Antennas Wireless Propag. Lett.*, vol. 13, pp. 919–992, 2014.
[11] J. He, X. Wang, L. Guo, S. Shen, and M. Lu, "A distributed retro-reflective beamformer for wireless power transmission," *Microw. Opt. Technol. Lett.*, vol. 57, no. 8, pp. 1873–1876, Aug. 2015.
[12] J. Bae, S.-H. Yi, H. Koo, S. Oh, H. Oh, W. Choi, J. Shin, C. M. Song, K. C. Hwang, K.-Y. Lee, and Y. Yang, "LUT-based focal beamforming system using 2-D adaptive sequential searching algorithm for microwave power transfer," *IEEE Access*, vol. 8, pp. 196024–196033, 2020.
[13] D. Belo, D. C. Ribeiro, P. Pinho, and N. Borges Carvalho, "A selective, tracking, and power adaptive far-field wireless power transfer system," *IEEE Trans. Microw. Theory Techn.*, vol. 67, no. 9, pp. 3856–3866, Sep. 2019.
[14] H. Koo, J. Bae, and Y. Yang, "A simple phase adaptation algorithm for compact microwave power transmitter array," in *Proc. IEEE Wireless Power Transf. Conf. (WPTC)*, Nov. 2020, pp. 342–345.
[15] J. Shin, J. Bae, H. Koo, S. Bae, J. Na, H. Oh, H. Jeon, H. Jung, Y. C. Choi, S. Woo, C. M. Song, K. C. Hwang, K.-Y. Lee, and Y. Yang, "5.8 GHz 4-channel beamforming Tx IC for microwave power transfer," *IEEE Access*, vol. 9, pp. 72316–72325, 2021.
[16] P. S. Yedavalli, T. Riihonen, X. Wang, and J. M. Rabaey, "Far-field RF wireless power transfer with blind adaptive beamforming for Internet of Things devices," *IEEE Access*, vol. 5, pp. 1743–1752, 2017.
[17] K. Hayashi, K. Aiura, Y. Tanaka, K. Kizaki, T. Fujihashi, S. Saruwatari, and T. Watanabe, "Curve fitting-based phase optimization for microwave power transfer," *IEEE Access*, vol. 10, pp. 23902–23912, 2022.
[18] A. Hajimiri, B. Abiri, F. Bohn, M. Gal-Katziri, and M. H. Manohara, "Dynamic focusing of large arrays for wireless power transfer and beyond," *IEEE J. Solid-State Circuits*, vol. 56, no. 7, pp. 2077–2101, Jul. 2021.
[19] R. Y. Miyamoto and T. Itoh, "Retrodirective arrays for wireless communications," *IEEE Microw. Mag.*, vol. 3, no. 1, pp. 71–79, Mar. 2002.
[20] R. Y. Miyamoto, Y. Qian, and T. Itoh, "A retrodirective array using balanced quasi-optical FET mixers with conversion gain," in *IEEE MTT-S Int. Microw. Symp. Dig.*, Anaheim, CA, USA, Jun. 1999, pp. 655–658.
[21] S. Mano and T. Katagi, "A method for measuring amplitude and phase of each radiating element of a phased array antenna," *Trans. IECE*, vol. J65-B, no. 5, pp. 555–560, May 1982.
[22] R. Sorace, "Phased array calibration," *IEEE Trans. Antennas Propag.*, vol. 49, no. 4, pp. 517–525, Apr. 2001.
[23] R. Long, J. Ouyang, F. Yang, W. Han, and L. Zhou, "Fast amplitude-only measurement method for phased array calibration," *IEEE Trans. Antennas Propag.*, vol. 65, no. 4, pp. 1815–1822, Apr. 2017.
[24] T. Takahashi, Y. Konishi, S. Makino, H. Ohmine, and H. Nakaguro, "Fast measurement technique for phased array calibration," *IEEE Trans. Antennas Propag.*, vol. 56, no. 7, pp. 1888–1899, Jul. 2008.
[25] T. Xie, J. Zhu, and J. Luo, "The simplified REV method combined with Hadamard group division for phased array calibration," *IEICE Trans. Commun.*, vol. E101.B, no. 3, pp. 847–855, 2018.
[26] G. A. Hampson and A. B. Smolders, "A fast and accurate scheme for calibration of active phased-array antennas," in *Proc. IEEE Antennas Propag. Soc. Int. Symp., USNC/URSI Nat. Radio Sci. Meeting*, 1999, pp. 1040–1043.
[27] S. D. Silverstein, "Application of orthogonal codes to the calibration of active phased array antennas for communication satellites," *IEEE Trans. Signal Process.*, vol. 45, no. 1, pp. 206–218, Jan. 1997.
[28] E. Lier, M. Zemlyansky, D. Purdy, and D. Farina, "Phased array calibration and characterization based on orthogonal coding: Theory and experimental validation," in *Proc. IEEE Int. Symp. Phased Array Syst. Technol.*, Boston, MA, USA, Oct. 2010, pp. 271–278.
[29] Y. Dong, S.-W. Dong, Y. Wang, and L. Gong, "Calibration method of retrodirective antenna array for microwave power transmission," in *Proc. IEEE Wireless Power Transf. (WPT)*, Perugia, Italy, May 2013, pp. 41–43.
[30] H. Koo, J. Bae, W. Choi, H. Oh, H. Lim, J. Lee, C. Song, K. Lee, K. Hwang, and Y. Yang, "Retroreflective transceiver array using a novel calibration method based on optimum phase searching," *IEEE Trans. Ind. Electron.*, vol. 68, no. 3, pp. 2510–2520, Mar. 2021.
[31] R. Long, J. Ouyang, F. Yang, Y. Li, K. Zhang, and L. Zhou, "Calibration method of phased array based on near-field measurement system," in *Proc. IEEE Antennas Propag. Soc. Int. Symp. (APSURSI)*, Jul. 2014, pp. 1161–1162.
[32] H. M. Aumann, A. J. Fenn, and F. G. Willwerth, "Phased array antenna calibration and pattern prediction using mutual coupling measurements," *IEEE Trans. Antennas Propag.*, vol. 37, no. 7, pp. 844–850, Jul. 1989.
[33] Y. Neidman, R. Shavit, and A. Bronshtein, "Diagnostic of phased arrays with faulty elements using the mutual coupling method," *IET Microw., Antennas Propag.*, vol. 3, no. 2, pp. 235–241, Mar. 2009.
[34] H. Pawlak and A. F. Jacob, "An external calibration scheme for DBF antenna arrays," *IEEE Trans. Antennas Propag.*, vol. 58, no. 1, pp. 59–67, Jan. 2010.
[35] S. Chen, S. Zhong, S. Yang, and X. Wang, "A multiantenna RFID reader with blind adaptive beamforming," *IEEE Internet Things J.*, vol. 3, no. 6, pp. 986–996, Dec. 2016.
[36] J. P. Gianvittorio and Y. Rahmat-Samii, "Fractal antennas: A novel antenna miniaturization technique, and applications," *IEEE Antennas Propag. Mag.*, vol. 44, no. 1, pp. 20–36, Feb. 2002.
[37] C. M. Song, S. Trinh-Van, S.-H. Yi, J. Bae, Y. Yang, K.-Y. Lee, and K. C. Hwang, "Analysis of received power in RF wireless power transfer system with array antennas," *IEEE Access*, vol. 9, pp. 76315–76324, 2021.

HYUNGMO KOO was born in Seoul, South Korea, in 1992. He received the Ph.D. degree from the Department of Electronic and Electrical Engineering, Sungkyunkwan University, Suwon, South Korea, in 2022.

He is currently an Engineer of Networks Business, Samsung Electronics Company Ltd., Suwon. His current research interests include the design of RF power amplifiers, digital pre-distortion techniques, RF transceiver arrays, and microwave power transfer systems.

JAEKYUNG SHIN was born in Seoul, South Korea, in 1993. He received the B.S. degree from the Department of Electronic and Electrical Engineering, Korea Aerospace University, Goyang, South Korea, in 2018. He is currently pursuing the Ph.D. degree with the Department of Electrical and Computer Engineering, Sungkyunkwan University, Suwon, South Korea.

His current research interests include the design of RF/mm-wave power amplifiers, efficiency enhancement techniques, broadband techniques, and microwave power transmission.

WOOJIN CHOI was born in Siheung, South Korea, in 1993. He received the B.S. degree from the Department of Electronic and Electrical Engineering, Sungkyunkwan University, Suwon, South Korea, in 2018, where he is currently pursuing the Ph.D. degree with the Department of Electrical and Computer Engineering.

His current research interests include the design of RF power amplifiers for basestations, broadband techniques, and MMICs.

SOOHYUN BIN was born in Seoul, South Korea, in 1996. He received the B.S. degree from the Department of Electronic and Electrical Engineering, Sungkyunkwan University, Suwon, South Korea, in 2022, where he is currently pursuing the Ph.D. degree with the Department of Electrical and Computer Engineering.

His current research interests include the design of RF/mm-wave power amplifiers, RF/analog integrated circuits, efficiency enhancement techniques, linearization techniques, broadband techniques, and microwave power transfer systems.

HANSIK OH was born in Seoul, South Korea, in 1991. He received the Ph.D. degree from the Department of Electronic and Electrical Engineering from Sungkyunkwan University, Suwon, South Korea, in 2022.

He is currently an Engineer of Networks Business, Samsung Electronics Company Ltd., Suwon. His research interests include the design of RF/mm-wave power amplifiers, RF/analog integrated circuit, efficiency enhancement techniques, linearization techniques, broadband techniques, and wireless power transfer systems.

HONGJUN LIM received the B.S. degree in electronics engineering from Sungkyunkwan University, Suwon, South Korea, in 2016. He is currently pursuing the combined Ph.D. and M.S. degree with the Department of Electronic and Electrical Engineering.

His research interests include analysis and design of miniaturized, array antennas, and near field measurement.

KANG-YOON LEE (Senior Member, IEEE) received the B.S., M.S., and Ph.D. degrees from the School of Electrical Engineering, Seoul National University, Seoul, South Korea, in 1996, 1998, and 2003, respectively.

Since 2012, he has been with the Department of Electrical and Computer Engineering, Sungkyunkwan University, South Korea, where he is currently an Associate Professor. His research interests include implementation of power integrated circuits, CMOS RF transceiver, analog integrated circuits, and analog/digital mixed-mode VLSI system design.

KEUM CHEOL HWANG (Senior Member, IEEE) received the B.S. degree in electronics engineering from Pusan National University, Busan, South Korea, in 2001, and the M.S. and Ph.D. degrees in electrical and electronic engineering from the Korea Advanced Institute of Science and Technology (KAIST), Daejeon, South Korea, in 2003 and 2006, respectively.

His research interests include advanced electromagnetic scattering and radiation theory and applications, design of multi-band/broadband antennas and radar antennas, and optimization algorithms for electromagnetic applications. He is a Life Member of KIEES and a member of IEICE.

YOUNGOO YANG (Senior Member, IEEE) was born in Hamyang, South Korea, in 1969. He received the Ph.D. degree in electrical and electronic engineering from the Pohang University of Science and Technology (POSTECH), Pohang, South Korea, in 2002.

From 2002 to 2005, he was at Skyworks Solutions Inc., Newbury Park, CA, USA, where he designed power amplifiers for various cellular handsets. Since March 2005, he has been with the Department of Electrical and Computer Engineering, Sungkyunkwan University, Suwon, South Korea, where he is currently a Professor. His research interests include RF/mm–wave power amplifiers, RF transmitters, and supply modulators.